Automated Calibration for Computerized Analysis of Prostate Lesions Using Pharmacokinetic Magnetic Resonance Images*

Pieter C. Vos, Thomas Hambrock, Jelle O. Barensz, and Henkjan J. Huisman

Department of Radiology, University Medical Centre Nijmegen, Netherlands
p.vos@rad.umcn.nl

Abstract. The feasibility of an automated calibration method for estimating the arterial input function when calculating pharmacokinetic parameters from Dynamic Contrast Enhanced MRI is shown. In a previous study [1], it was demonstrated that the computer aided diagnoses (CADx) system performs optimal when per patient calibration was used, but required manual annotation of reference tissue. In this study we propose a fully automated segmentation method that tackles this limitation and tested the method with our CADx system when discriminating prostate cancer from benign areas in the peripheral zone.

A method was developed to automatically segment normal peripheral zone tissue (PZ). Context based segmentation using the Otsu histogram based threshold selection method and by Hessian based blob detection, was developed to automatically select PZ as reference tissue for the per patient calibration.

In 38 consecutive patients carcinoma, benign and normal tissue were annotated on MR images by a radiologist and a researcher using whole mount step-section histopathology as standard of reference. A feature set comprising pharmacokinetic parameters was computed for each ROI and used to train a support vector machine (SVM) as classifier.

In total 42 malignant, 29 benign and 37 normal regions were annotated. The diagnostic accuracy obtained for differentiating malignant from benign lesions using a conventional general patient plasma profile showed an accuracy of 0.65 (0.54-0.76). Using the automated segmentation per patient calibration method the diagnostic value improved to 0.80 (0.71-0.88), whereas the manual segmentation per patient calibration showed a diagnostic performance of 0.80 (0.70-0.90).

These results show that an automated per-patient calibration is feasible, a significant better discriminating performance compared to the conventional fixed calibration was obtained and the diagnostic accuracy is similar to using manual per-patient calibration.

1 Introduction

Several studies have indicated that multimodal MRI increases the prostate cancer (PCa) localization accuracy of the radiologist. The accuracy is, however,

dependent on the experience of the radiologist [2,3,4]. To help improve the diagnostic accuracy of the (unexperienced) radiologist, we are investigating the possible additional value of CADx. Previously [1], the feasibility was demonstrated of an in-house developed CADx system that calculates the malignancy likelihood of a given suspicious area in the peripheral zone of the prostate using T1-w DCE-MRI at 1.5T. Discrimination of malignant and benign regions was performed using a SVM as classifier that was trained with features extracted from quantitative pharmacokinetic (PK) maps as well as T1 estimates. The study showed that a diagnostic accuracy of 0.83 (0.75-0.92) was obtained by a standalone CADx, which is comparable to an expert radiologist performance.

Pharmacokinetic (PK) DCE-MRI could further improve PCa differentiation by reducing inter patient and inter MR scanner fluctuations compared to conventional DCE-MRI. PK tissue parameters are estimated by fitting a tracer physiologic compartment model to the observed DCE-MRI data that is driven by a plasma profile. Various techniques for estimating plasma profiles exist. Quite some PK estimators do not include per patient calibration, but use a general patient plasma profile (fixed calibration) [5,6]. Huisman et al. [7] demonstrated that the plasma profile varies per patient and thus, fixed calibration can cause fluctuation among patient when estimating the PK parameters. In [8], it was shown that the CADx system performs significantly better using per patient calibration instead of fixed calibration. The presented method was, however, dependent on manual annotation of healthy tissue before a malignancy likelihood could be calculated. This study addresses that limitation by presenting a more objective and automated calibration method and investigates its effect on the diagnostic accuracy of the CADx system.

The purpose of this study was to investigate the feasibility of a CADx system capable of objectively discriminating PCa from non-malignant disorders located in the peripheral zone of the prostate using an automated per patient calibration method.

2   Method

2.1   Pharmacokinetic Modeling

Analysis of DCE-MRI data requires knowledge of the concentration of the contrast agent in the blood plasma. Without calibration (or fixed calibration), interpatient plasma profile variability causes fluctuations in PK estimates, which are not related to the tissue condition. When using a power injector the most likely cause of differences in plasma curves are differences in body weight (total distributional volume), heart rate, vascular condition. Removing the plasma shape can be regarded as a form of patient calibration whereas fixed calibration uses a fixed plasma function over all patients.

The parametric model for analyzing contrast agent concentration time curves in DCE-MRI is the two compartment model of Tofts et al. [9]. The observed concentration-time curve can be expressed as:

$$C_v(t) = h(t; t_0, V_e, K^{trans}, Washout) \otimes C_p(t), \tag{1}$$

where $C_v(.)$ denotes the observed tracer concentration, $h(.)$ the tissue impulse response, $C_p(t)$ the plasma input function and $t_0, V_e, K^{trans}, Washout$ are parameters from the model. The reference tissue method estimates the plasma input function by:

$$\hat{C}_p(t) = C_{ref,v}(t)/h_{ref,v}(t), \tag{2}$$

where $C_{ref,v}(.)$ represents the observed plasma profile for tissue v and $h_{ref,v}(.)$ a reference plasma profile for tissue v based on literature. The reference tissue method is considered to be a robust technique [10].

2.2   Automated Per Patient Calibration

In a previous study [8], it was demonstrated that using PZ as reference tissue gave good results for estimating PK parameters. In this study a method was developed to auto segment PZ. The method is divided into two stages. First, the location of the prostate is detected using a blob detection method. In the second stage, this location is further refined to segment a PZ region.
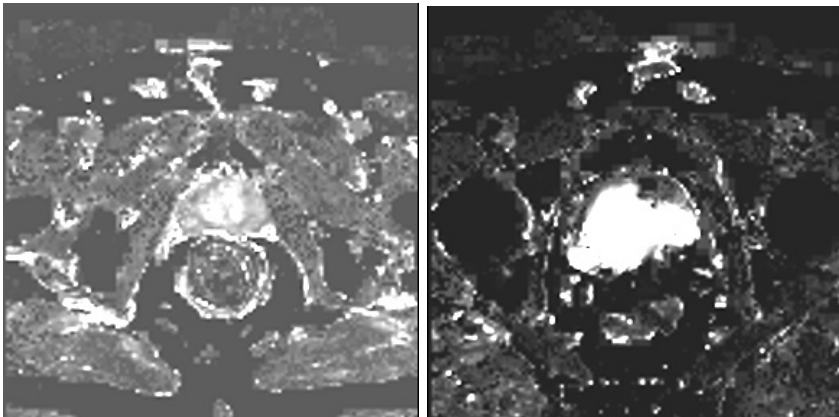
(a) DCE of the prostate area.   (b) DCE of the bladder area.

Fig. 1. Rational for modeling an early and large enhancing blob in the pelvic area

Automated Localization of the Prostate. The prostate can be modelled as a large enhancing area (or blob) in the pelvis. Figure 1(a) demonstrates this model where the prostate can easily be detected by a human observer. Large and strong enhancements can be observed in the transition zone of the prostate making it suitable for detection. First experimental results showed however, that this assumption is not only true for the prostate. Because the acquisition time for the DCE-MRI can be rather long (3 min), contrast agent also arrives in the bladder, resulting in a comparably large enhancing blob, as demonstrated in figure 1(b). The prostate model is therefore extended by including the arrival time of the contrast agent (t_0 of $C_v(t)$). Otsu's automatic threshold selection

method from gray-level histograms ([11]) is used to segment early enhancing structures in the relative enhancement image $V(x)$:

$$V_O\left(\mathbf{x}\right) = \begin{cases} V(\mathbf{x}), & t_0(x) < th_{Otsu} \\ 0 \end{cases} \tag{3}$$

A common approach to detect blobs is to consider the Taylor expansion of V_O at multiscale for a given neighborhood of pixel x [12],

$$V_O\left(\mathbf{x} + \delta\mathbf{x}, \sigma\right) \approx V_O(\mathbf{x}, \sigma) + \delta\mathbf{x}^T \nabla_\sigma + \delta\mathbf{x}^T H_\sigma \delta\mathbf{x}, \tag{4}$$

where ∇_σ and H_σ are the gradient vector and Hessian vector of an image at scale σ. Here, V_O is convolved using derivatives of Gaussians:

$$\frac{\delta}{\delta\mathbf{x}} V_O(\mathbf{x}, \sigma) = \sigma V_O(\mathbf{x}) \frac{\delta}{\delta\mathbf{x}} G(\mathbf{x}, \sigma). \tag{5}$$

Next, from H_σ eigenvalues $\lambda_{\sigma,k}$ are computed, corresponding the the k-th normalized vector $\hat{u}_{\sigma,k}$ and analyzed to determine the likelihood of a pixel $\mathbf{x}$ belonging to a blob. This analysis is based on the following likelihood function (for bright blob, dark background):

$$P(\mathbf{x}, \sigma) = |\lambda_1(x)||\lambda_2(x)||\lambda_3(x)|, \tag{6}$$

that is, all three eigen values should be large to represent a blob. A multiscale approach is adopted after which the maximum response is selected:
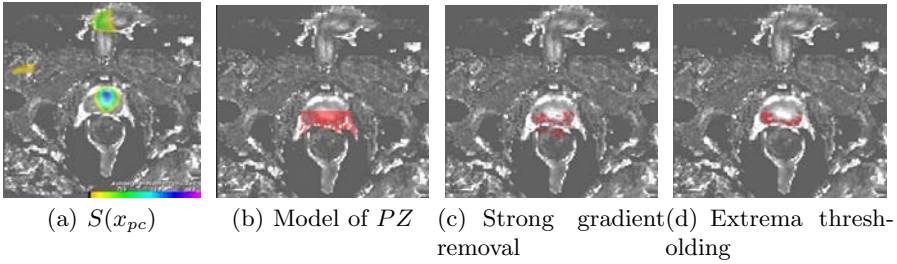
$$P(\mathbf{x}) = \max_{\sigma_{min} \leq \sigma \leq \sigma_{max}} P(\mathbf{x}, \sigma). \tag{7}$$

The center location of the prostate x_{pc} containing the highest probability is then selected by $x_{pc} = arg\max_x P(\mathbf{x})$. In figure 2(a) a probability map is shown that is used for the prostate detection.

Automated Segmentation of Normal Peripheral Zone Tissue. In the second stage of the method, a context based segmentation is performed to extract normal peripheral zone tissue. The method is based on the model that the PZ is mainly dorsal located of x_{pc}. Thus, we define a box-mask below x_{pc} with height, width and depth set to σ to mask V_O. Here, σ corresponds with the size of the prostate and is the scale at which $P(x_{pc})$ was found by the blob detector:

$$S(x_{pc}) = arg\max_\sigma (P(x_{pc}, \sigma) \tag{8}$$

Figure 2(b) demonstrates this model. Simple thresholding of extrema and removal of sharp edges using a gradient magnitude filter can now be applied to the box-mask which results in the segmentation of normal peripheral zone tissue, as demonstrated in figures 2(c) and 2(d).

(a) $S(x_{pc})$ (b) Model of PZ (c) Strong   gradient (d) Extrema thresh-
                                              removal   olding

Fig. 2. Example case of context based segmentation of normal peripheral zone tissue

2.3   CADx Performance Evaluation

The features K^{trans}, V_e and $Washout$ were computed and used to train a SVM
as classifier [9]. The features were combined into a single malignancy likelihood
estimate using the SVM. The output of the classifier was used as a measure of
likelihood of malignancy. The discriminating performance of the CADx system
was estimated by means of the area under the receiver operator characteristics
(ROC) curve (AUC). The prospective performance of the lesion analysis with
per patient and fixed calibration were estimated by means of leave-one-patient-
out (LOPO) cross validation. LOPO avoids training and testing on the same
data and to emphasize the prospective value, one whole patient case was drawn
from the set. The LOPO involves training on all but one case, estimating the
likelihood of that left-out case, and repeating the procedure until each case has
been tested individually. The bootstrap technique was used to compute 95% con-
fidence intervals for the AUC and significance level for the paired difference [13].

2.4   Experiment

The study set consisted of 38 consecutive patients that were selected between
January 2007 and October 2008. These patients had biopsy-proven PCa and un-
derwent dynamic contrast-enhanced MR imaging at 3.0T, complementary to the
routine staging MR imaging examination of the prostate. Patients were included
in the study only if they were candidates for radical retropubic prostatectomy
within 6 weeks after MR imaging. The study was approved by the institutional
review board, and informed consent was obtained from all patients prior to MR
imaging. Exclusion criteria were: previous hormonal therapy, lymph nodes pos-
itive for metastases at frozen section analysis, contraindications to MR imaging
(e.g., cardiac pacemakers, intracranial clips), contraindications to endorectal coil
insertion (e.g., anorectal surgery, inflammatory bowel disease).

Images were acquired with a 3.0T whole body MR scanner (TrioTim, Siemens
Medical Solutions, Erlangen, Germany). A pelvic phased-array as well as a
balloon-mounted disposable endorectal surface coil (MedRad®, Pittsburgh, PA,
USA) inserted and inflated with approximately 80 cm^3 of Perfluorocarbon
(FOMBLIN LC08), were used for receiving. The machine body coil was used for

RF transmitting. An amount of 1 mg of glucagon (Glucagon®, Novo Nordisk, Bagsvaerd, Denmark)) was administered directly before the MRI scan, to all patients to reduce peristaltic bowel movement during the examination.

High-spatial-resolution T2-weighted fast spin-echo imaging in the axial, sagittal and coronal planes, covering the prostate and seminal vesicles, was performed. 3D T1-weighted spoiled gradient echo images were acquired before and during an intravenous bolus injection of paramagnetic gadolinium chelate (0.1 mmol/kg, gadopentetate, Magnevist®; Schering, Berlin, Germany) using a power injector (Spectris, Medrad®, Pittsburgh, PA, US) with an injection rate of 2.5 ml/second followed by a 15 ml saline flush for 300 sec every 3 seconds. Fitting the DCE-MRI is decribed elsewhere [14].

Whole-mount step-section histology tumor maps were used as ground truth for annotating PCa (with a relevant diameter of at least 5mm), non-malignant suspicious enhancing (NS) and normal (N) regions on T2-w images for all patients in consensus by two readers.

3   Results

One patient case was excluded because the DCE examination had failed. In total 42 malignant regions were annotated in the peripheral zone. The number of NS regions annotated in the peripheral zone was 29. The number of normal peripheral zone regions was 38.

The effect of the per patient calibration on the diagnostic performance was first evaluated by pairwise scatterplots of PK parameters of the lesions. It is noticeable in figure 3(a) that without calibration the clusters overlap more than the clusters in figure 3(c) where manual calibration is included. Figure 3(b) shows similar results for automatic patient calibration. Furthermore, the N and NS

(a) Fixed   (b) Auto   (c) Manual
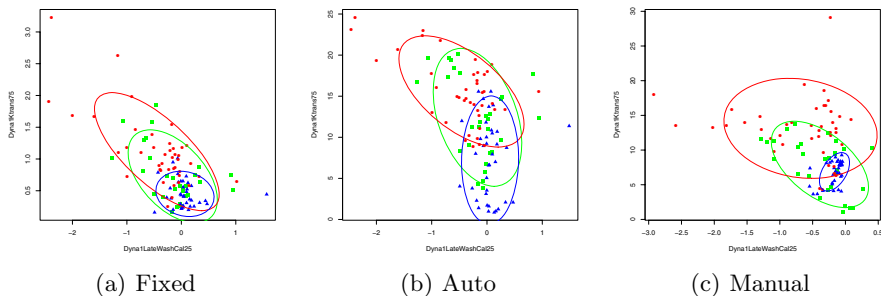
Fig. 3. Pairwise scatterplots of 2 kinetic parameters, $Washout$ versus K^{trans}, for the whole database with squares representing NS regions, spheres as malignant regions and triangles as N regions for the different calibration methods used. The ellipsoids summarize the three clusters by fitting a bivariate normal distribution and displaying the outline at 2 times standard deviation radius. It is noticeable that the clusters overlap one another when fixed calibration is used, whereas manual and automated per patient calibration demonstrate a noticeable clustering of features.
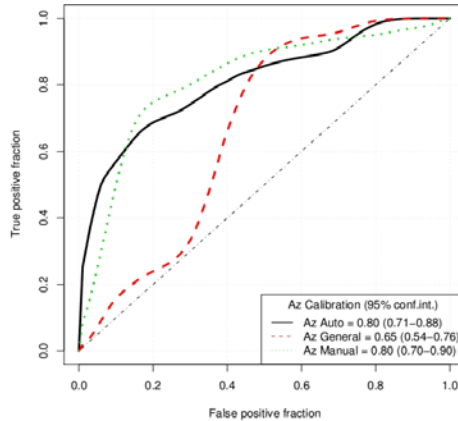
Fig. 4. ROC curves showing the discriminating performance of the CADx system using the different calibration methods fixed, automated per patient and manual per patient calibration

clusters have a smaller covariance when patient calibration is used. An effect on the diagnostic performance can therefore be expected. The different distributions demonstrate the strong effect of the chosen calibration method.

The performance of discriminating malignant lesions from NS areas with fixed, manual and automatic calibration is demonstrated in the ROC curves shown in figure 3. Here, the focus is on the characterization of NS and malignant regions, because it is more challenging and clinically relevant. The diagnostic accuracy was 0.65 (95% confidence intervals = 0.54-0.76)) when fixed calibration was used. The diagnostic accuracy improved significantly for both manual per patient calibration, Az=0.80 (0.70-0.90), as for automated per patient calibration, Az=0.80 (0.71-0.88). The marginal difference between the automated and manual calibration means that they perform similar, which was the intended goal.

4   Conclusion

In this study, we have demonstrated the feasibility of an automated calibration method for estimating the arterial input function when calculating pharmacokinetic parameters from DCE-MRI. The results show a significant better discriminating performance (Az=0.80 (0.71-0.88)) compared to the conventional fixed calibration. The performance is similar to using the manual per patient calibration.

References

1. Vos, P., Hambrock, T., Hulsbergen-van de Kaa, C., Fütterer, J., Barentsz, J., Huisman, H.: Computerized analysis of prostate lesions in the peripheral zone using dynamic contrast enhanced MRI. Med. Phys. 35(3), 888–899 (2008)
2. Hricak, H., Choyke, P., Eberhardt, S., Leibel, S., Scardino, P.: Imaging prostate cancer: a multidisciplinary perspective. Radiology 243(1), 28–53 (2007)

3. Fütterer, J., Heijmink, S., Scheenen, T., Veltman, J., Huisman, H., Vos, P., de Kaa, C., Witjes, J., Krabbe, P., Heerschap, A., Barentsz, J.: Prostate Cancer Localization with Dynamic Contrast-enhanced MR Imaging and Proton MR Spectroscopic Imaging. Radiology 241(2), 449–458 (2006)
4. Chan, I., Wells, W., Mulkern, R., Haker, S., Zhang, J., Zou, K., Maier, S., Tempany, C.: Detection of prostate cancer by integration of line-scan diffusion, T2-mapping and T2-weighted magnetic resonance imaging; a multichannel statistical classifier. Med. Phys. 30(9), 2390–2398 (2003)
5. Weinmann, H.J., Laniado, M., Mutzel, W.: Pharmacokinetics of GdDTPA/ dimeglumine after intravenous injection into healthy volunteers. Physiol. Chem. Phys. Med. NMR 16(2), 167–172 (1984)
6. Brix, G., Semmler, W., Port, R., Schad, L.R., Layer, G., Lorenz, W.J.: Pharmacokinetic parameters in CNS Gd-DTPA enhanced MR imaging. J. Comput. Assist. Tomogr. 15(4), 621–628 (1991)
7. Huisman, H., Veltman, J., Boetes, C., Karssemeijer, N., Blickman, H., Barentsz, J.: Computer-aided diagnosis of breast MRI using pharmacokinetic modeling. RSNA, SSC17–09 (2006)
8. Vos, P.C., Hambrock, T., Fütterer, J.J., van de Kaa, C.A.H., Barentsz, J., Huisman, H.H.: Effect of calibration on computerized analysis of prostate lesions using quantitative dynamic contrast-enhanced magnetic resonance imaging. In: SPIE, vol. 6514, 65140U (2007)
9. Tofts, P., Brix, G., Buckley, D., Evelhoch, J., Henderson, E., Knopp, M., Larsson, H., Lee, T., Mayr, N., Parker, G., Port, R., Taylor, J., Weisskoff, R.: Estimating kinetic parameters from dynamic contrast-enhanced $T(1)$-weighted MRI of a diffusable tracer: standardized quantities and symbols. J. Magn. Reson. Imaging 10(3), 223–232 (1999)
10. Kovar, D., Lewis, M., Karczmar, G.: A new method for imaging perfusion and contrast extraction fraction: input functions derived from reference tissues. J. Magn. Reson. Imaging 8(5), 1126–1134 (1998)
11. Otsu, N.: A threshold selection method from gray-level histograms. EEE Trans. Sys., Man., Cyber. 9(1), 62–66 (1979)
12. Frangi, A.F., Niessen, W.J., Vincken, K.L., Viergever, M.A.: Multiscale vessel enhancement filtering. In: Wells, W.M., Colchester, A.C.F., Delp, S.L. (eds.) MICCAI 1998. LNCS, vol. 1496, p. 130. Springer, Heidelberg (1998)
13. Rutter, C.: Bootstrap estimation of diagnostic accuracy with patient-clustered data. Acad. Radiol. 7(6), 413–419 (2000)
14. Hittmair, K., Gomiscek, G., Langenberger, K., Recht, M., Imhof, H., Kramer, J.: Method for the quantitative assessment of contrast agent uptake in dynamic contrast-enhanced MRI. Magn. Reson. Med. 31(5), 567–571 (1994)